

# Precisely position- and angular-controllable optical trapping and manipulation via a single vortex-pair beam

Jisen Wen,\* Binjie Gao,\* Dadong Liu, Guiyuan Zhu, and Li-Gang Wang

*Department of Physics, Zhejiang University, Hangzhou 310027, China<sup>†</sup>*

(Dated: November 5, 2021)

Optical trapping and manipulation using structured laser beams now attract increasing attention in many areas including biology, atomic science, and nanofabrication. Here we propose and experimentally demonstrate the use of a single vortex-pair beam in optical trapping and manipulation. Using the focal properties of such vortex-pair beams, we successfully manipulate two spherical microparticles simultaneously, and obtain the precise position-control on the microparticles by adjusting the off-axis parameter  $a$  of the vortex-pair beam in its initial phase plane. Furthermore, the high-precision angular-controllable rotation of cylindrical microrods is also achieved at will by rotating the initial phase structure of such vortex-pair beams, like an optical wrench due to two focused bright spots at the focal plane of objective lens. Our result provides an alternative manipulation of microparticles and may have potential applications in biological area, and optically driven micromachines or motors

PACS numbers: 42.65.Jx, 41.85.-p, 42.60.Jf, 42.25.-p, 42.25.Bs, 42.40.Eq, 42.62.-b

## I. INTRODUCTION

Optical trapping and manipulation have been widely used in a variety of areas including atom cooling [1, 2], molecular biology [3], nanotechnology [4, 5], as well as other disciplines. Ashkin pioneered the investigation on optical force produced by a laser beam in 1970 [6]. In 1986, Ashkin *et al.* realized optical trapping of dielectric particles by the gradient force from a single beam, which is named as optical tweezers [7]. Since then, optical tweezers become a powerful and flexible tool for trapping and manipulating the micrometre-sized objects. More importantly, optical tweezers have many new progress, such as holographic optical tweezers (HOTs) [8–11], three-dimensional trapping of microparticles [12], transportation of the micro-objects in the air [13], and surface plasmon-based nano-optical tweezers [14]. The usual method of trapping microparticles often uses the gradient force of a focused Gaussian beam. With the invention of new kinds of both scalar and vectorial optical beams, many structured light beams are applied to optical trapping, like Laguerre-Gaussian beams [15–17], Bessel beams [18, 19], partially coherent light beams [20], Airy beams [21], helico-conical beams [22], radially polarized beams [23], cylindrical vector beams [24], and Poincaré beams [25]. In addition, not only structured beams but also pulsed light can be used to trap linear microparticles [26–28] and nonlinear microparticles [29, 30].

In many applications, it is required to manipulate the position of trapped microparticles or rotate them. In 2001, Dufresne *et al.* designed the arrays of HOTs for trapping hundreds of particles simultaneously and the position of trap is controllable [9]. This method is also applied to manipulate the position of neutral atoms [31]. Leonardo *et al.* also proposed an iterative algorithm to make holograms for generating optical traps for arbitrary three-dimensional trapping [32]. Meanwhile, vortex beams always rotate microparticles due to their orbital angular momentum, however, this rotation cannot be well suppressed and well controlled [33]. Additionally, rotating the spiral interference pattern by an interferometer of high accuracy [34] or a rectangular aperture inserted in the beam axis [35] can also rotate microparticles. Moreover, Zhang *et al.* have theoretically proposed optical doughnuts for rotating microparticles by rotating a modified vortex phase [36].

On the other hand, as the shape complexity of microparticles increases, like cylindrical microrods, trapping and rotating these microparticles become more difficult. Cylindrical microrods have been used in practical applications such as scanning optical probes in force microscope [37] and the fabrication of nanoelectronic devices [38]. Consequently, there has been also increasing interest in the trapping of cylindrical microrods. For instance, Gauthier *et al.* have experimentally observed that cylinders can be manipulated and rotated in the transverse plane about the optical axis [39]. Other approaches including using a dual-beam fiber trap with one non-rotationally symmetric trapping beam [40], a line optical trap [41], and shape-induced optical forces [42] have been used to manipulate micro-sized objects

\*J. S. Wen and B. J. Gao contributed equally to this work.

<sup>†</sup>Electronic address: sxwlg@yahoo.com

like cylinders or nanowires. Although HOTs exhibit great advantages for precisely rotating the cylinders [43, 44], the novel methods for effectively trapping of the non-spherical particles are still expected in new practical applications.

The vortex-pair beam, a kind of structured light fields, contains a pair of vortices at the initial phase plane, and it was earlier studied analytically on its propagation in free space by Guy in 1993 [45]. Sometimes, vortex-pair beams, containing opposite-charged vortices, are also known as vortex-dipole beams. Later, the annihilation phenomenon of vortex dipoles has been discussed by Chen *et al.* [46]. The vortex-dipole beams propagating in various optical systems, for example, an astigmatic lens [47, 48], a high numerical-aperture system [49, 50] and half-plane [51, 52], have also been investigated. It is also worth mentioning that the vortex-pair beam of electrons has been experimentally realized by nanofabricated hologram grating in 2013 [53]. Although these works related to the evolution properties of the vortex-pair beams have been investigated, the application of the vortex-pair beams in optical trapping has never been realized yet.

In this work, we have experimentally realized the stable trapping of spherical microparticles and cylindrical microrods based on a single vortex-pair beam with two positive topological charges. It shows that the precise control of spherical microparticles with their positions in one direction can be realized. We have also demonstrated the controllable rotation of cylindrical microrods by externally rotating the vortex-pair beam. To the best of our knowledge, it is the first time to adopt a vortex-pair beam to realize the controllable trapping and manipulation of the micrometre-sized objects. This method could provide a high-precision and reliable control on the trapping of microparticles and is potentially useful for many other areas.

## II. THEORETICAL DESCRIPTION

First, let us introduce the description of such vortex-pair beam. In experiments, one can pass a Gaussian beam to be incident on a designed phase plate with a pair of vortices. The light field at the initial plane can be expressed as,

$$E_i(u, v) = G_0 \exp\left(-\frac{u^2 + v^2}{w_0^2}\right) \phi(u, v), \quad (1)$$

where  $G_0$  is a constant related to the input power of light,  $w_0$  is the beam width of the incident Gaussian beam,  $(u, v)$  are the Cartesian coordinates at the initial plane and  $\phi(u, v)$  is the initial pure phase function of the vortex-pair phase given by

$$\phi(u, v) = \left[\frac{u - a + iv}{\sqrt{(u - a)^2 + v^2}}\right]^{m_1} \left[\frac{u + a + iv}{\sqrt{(u + a)^2 + v^2}}\right]^{m_2}, \quad (2)$$

where  $m_{1,2}$  are the integer topological charges of two vortices, and  $a$  is the initial off-axis distance of each vortex. Note that the vortex-pair phase is not rotationally symmetric, which is different from a single integer vortex beam. When light propagates in a linear optical system, under the paraxial approximation, the output field can be calculated by the following Collins formula [54, 55]

$$E_o(x, y, z) = \frac{\exp(ikL)}{i\lambda B} \iint_{-\infty}^{+\infty} E_i(u, v) \exp\left\{\frac{ik}{2B} \times [A(u^2 + v^2) + D(x^2 + y^2) - 2(ux + vy)]\right\} du dv, \quad (3)$$

where  $A$ ,  $B$ , and  $D$  are the elements of a  $2 \times 2$  ray transfer matrix  $\begin{pmatrix} A & B \\ C & D \end{pmatrix}$  describing the total linear optical system from the input to output planes,  $L$  is the eikonal along the propagation axis, and  $k = 2\pi/\lambda$  is the wave number of light. It is hard to obtain the analytical result, thus we have numerically solved Eq. (3) by using the trapezoidal numerical integration, which can be directly performed on MATLAB software. In order to make sure the output fields correct, the discretization of the integrand function (its main part is the initial field expressed by Eq. (3)) has the small integral intervals, taking 1000 sampling data within the range of  $(-5w_0, 5w_0)$  in the  $x$  and  $y$  directions, respectively, and there are total  $10^6$  sampling points in the initial plane. The requirement of the discretization procedure is to obtain the stable solution of the output field with high precision, and the relative error in our calculation is controlled to be smaller than  $10^{-6}$ , which is sufficient to present correctly the field evolution in the focused optical system.

## III. RESULTS AND DISCUSSIONS

We use this kind of beams to trap and manipulate microparticles, and the experimental setup is shown in Fig. 1(a). The initial Gaussian beam with the wavelength  $\lambda = 533$  nm is incident on a phase-only spatial light modulator

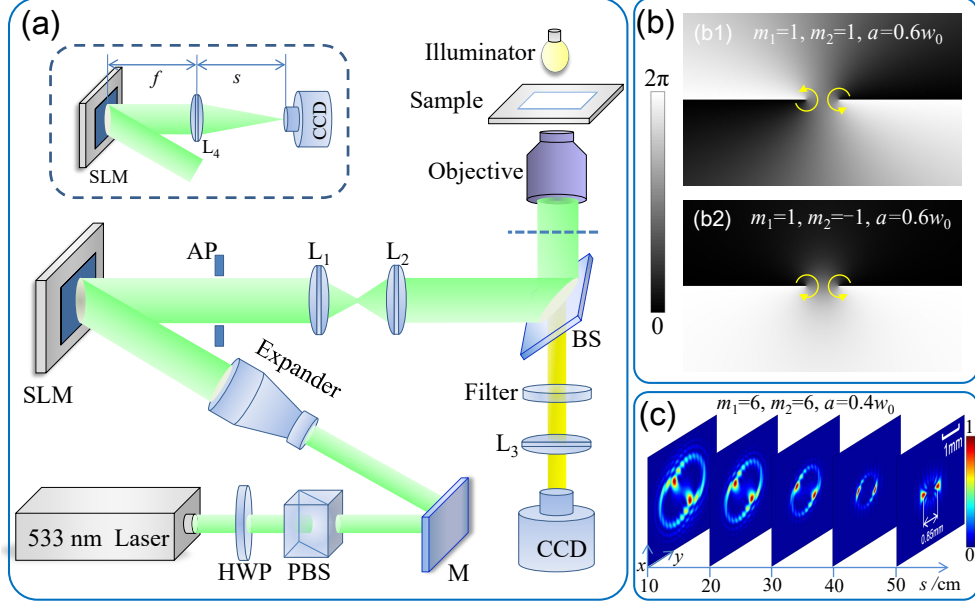


FIG. 1: (a) Schematic of optical trapping system. Notations are: HWP, half-wave plate; PBS, polarized beam splitter; SLM, spatial light modulator; AP, Aperture; BS, beam splitter; M, mirror; L, lens. The dash line below the objective lens represents the position where we have measured the power of the incident beam. The left-top inset in (a) shows the propagation of the vortex-pair beams in a 2- $f$  lens system with the focal length  $f = 50$  cm, which is used to explore the focal property of such beams by changing  $s$ . (b) Two examples of vortex-pair phase with different topological charges (b1, top)  $m_1=1, m_2=1$  and (b2, bottom)  $m_1=1, m_2=-1$ . (c) Numerical results for the evolution of the vortex-pair beam at different  $s$  under the parameters  $m_1=6, m_2=6, a=0.4w_0$  in a 2- $f$  system as shown in the inset of (a). Note that in our experiment the laser is expanded to have  $w_0 = 1.5$  mm before the SLM, and  $s$  in the inset of (a) is the distance from the lens to the CCD.

(SLM, Holoeye Pluto-2-VIS-056) with high resolution ( $1920 \times 1080$  pixel) and  $8 \mu\text{m}$  pixel pitch, which acts as a phase diffractive optical element. The incident Gaussian beam is expanded by the expander, and the beam width  $w_0$  is enlarged to be  $w_0 = 1.5$  mm which is measured by a camera-based laser beam profiler (Ophir, SP928 Beam Profiling Camera). The beam waist  $w_0 = 1.5$  mm is also used in numerical calculation. The polarized beam splitter combined with the half-wave plate is to realize the horizontal polarization and the controllable power of the laser beam. Here the phase pattern on the SLM needs to be corrected due to the imperfect flatness of SLM's surface and the wavefront of incident beam. We have set the aberration correction function to generate the background compensation image by using the SLM pattern generator software at the beginning of experiment. We would also like to emphasize that in our experiment, the blazed grating phase (also known as prism phase) is applied on the SLM which can also be directly generated by the Holoeye SLM pattern generator software. The parameters of the blazed grating phase can be set by the software and the external designed vortex-pair phase distribution like Fig. 1(b) is loaded independently. The more detail operations can be found on the manual book of the SLM [56]. Two examples of the vortex-pair phase with topological charges  $m_1 = m_2 = 1$  and  $m_1 = -m_2 = 1$  are shown in Fig. 1(b). The modulated first-order diffraction beam, which is the vortex-pair beam, is selected by an aperture. The vortex-pair beam then goes through an objective lens ( $\times 100$ , NA=1.25; or  $\times 40$ , NA=0.6) and is focused on the sample which is placed on a three-dimensional adjustable platform. The trapping system is configured with the vortex-pair beam directed upwards, which allows easier access to realize adjustable platform. The sample is illuminated by a white-light source from the top and is imaged onto a CCD camera. The filter is used to block the green light reflected or scattered back from the cover slip which has high intensity during the stable trapping process.

Figure 2 shows the trapping and manipulation of spherical microparticles using the vortex-pair beam. Here the polystyrene spheres (with diameter  $d_p = 1 \mu\text{m}$  [57]) are used as the probe samples in this experiment. It is worth to mention that the power of the incident vortex-pair beam to the objective lens is about 20 mW. It is observed from Fig. 2(a) that in the case of the vortex-pair beam with positive topological charges  $m_1 = 6, m_2 = 6$ , two spherical microparticles are trapped in the horizontal direction simultaneously. It could be understood by Fig. 1(c) that when the vortex-pair beam is focused by an objective lens, there exists two bright spots at the focal plane, which can directly trap two microparticles. When the parameter  $a$  contained in the SLM phase structure is adjusted, the position of the trapped spherical microparticles is also changed. For instance, the separation distance  $d_s$  of the two trapped spherical microparticles is  $3.92 \mu\text{m}$  with  $a = 0.3w_0$  as shown in Fig. 2(a1), while it decreases to  $1.64 \mu\text{m}$

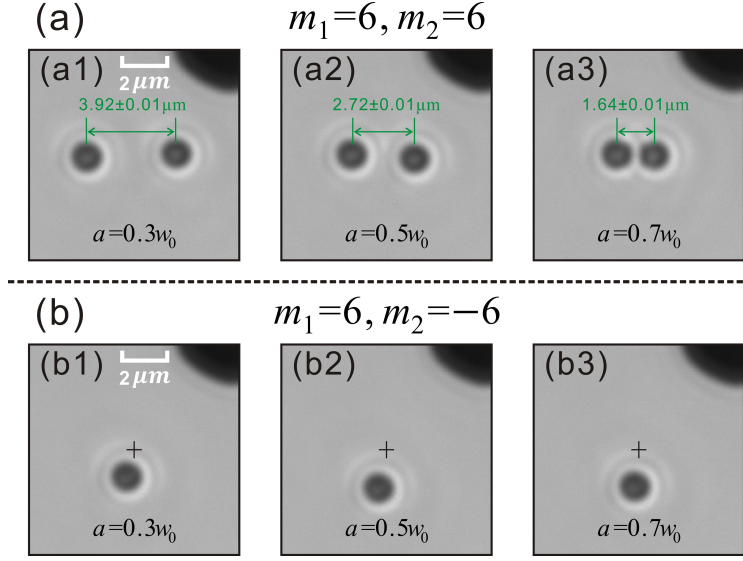


FIG. 2: Camera snapshots of spherical microparticles inside the optical trap induced by the focused vortex-pair beam with different topological charges (a)  $m_1 = 6, m_2 = 6$  and (b)  $m_1 = 6, m_2 = -6$ , through adjusting the off-axis parameter (a1, b1)  $a = 0.3w_0$ , (a2, b2)  $a = 0.5w_0$ , (a3, b3)  $a = 0.7w_0$  in their initial phase structures. Here  $w_0 = 1.5$  mm, and the diameter of polystyrene microparticles  $d_p = 1\mu\text{m}$ . Note that the shadow on the right-top corner is one of the scale marks on the glass slide, and the cross symbol in (b) is just for the convenient observation on the position of the single microparticle.

under  $a = 0.7w_0$  displayed in Fig. 2(a3). It seems that the larger  $a$  is, the closer the separation  $d_s$  of two trapped spherical microparticles is. Therefore, one can precisely control the distance between two interested microparticles by this method. However, in the case of  $m_1 = 6, m_2 = -6$ , it is seen in Fig. 2(b) that only one spherical microparticle is trapped as compared with the case of  $m_1 = 6, m_2 = 6$ . Furthermore, adjusting  $a$  makes no clear difference on the trapping results, except for a slight change of the microparticle's position.

Figure 3 further shows the dependence of the separation distance  $d_s$  between two trapped spherical microparticles on the control parameter of the off-axis distance  $a$  in the initial vortex-pair phase. Here, we used the polystyrene microspheres with diameter  $d_p = 1\mu\text{m}, 0.5\mu\text{m}$  [57]. When the vortex-pair beam has two positive topological charges, for example, in the case of  $m_1 = m_2 = 6$ , the vortex-pair beam can be focused into two bright spots as shown in Fig. 1(c) (at  $s = f = 50$  cm). These two bright spots with high intensity peaks lead to the strong transverse gradient forces for trapping microparticles. Thus two spherical microparticles are trapped, as shown in Figs. 2(a1) to 2(a3). The separation distance  $d_s$  between these two microparticles can be manipulated precisely by changing the value of  $a$ . For large-size microparticles of the cases in Figs. 3(a) and 3(b), whatever the power is, for examples when  $P = 20$  mW and  $P = 40$  mW (we have also measured the effect under other incident power), the separation distance  $d_s$  between the two trapped microparticles decreases linearly as  $a$  increases, and such linearity of  $d_s$  vs  $a$  keeps very well for those microparticles with  $d_p = 1\mu\text{m}, 2\mu\text{m}$ , and  $3\mu\text{m}$ . For the experimental results for  $d_p = 2\mu\text{m}$ , and  $3\mu\text{m}$  are not presented here since the results are similar. However, in Fig. 3(c), we have also observed the clear deviation of  $d_s$  from the linearity vs  $a$  under different incident power when we used the smaller particles with  $d_p = 0.5\mu\text{m}$ . From Fig. 3(c), as the incident power  $P$  decreases, from 43 mW to 22 mW, under the same conditions of other parameters, the deviation from the linearity of the value  $d_s$  vs  $a$  is more significant around the value of  $a = 0.8w_0$ , especially for  $P = 22$  mW. The experiment measurement for such smaller sized microparticles cannot be performed under the lower power because the microparticles will escape from the optical trap for the lower power. We think that such deviation phenomenon is due to the influence of the optical binding effect between two microparticles [58, 59]. All the experimental data are measured from the images like Figs. 2(a1) to 2(a3) in different cases of  $m_1 = m_2 = 6$ ,  $m_1 = m_2 = 8$ , and  $m_1 = m_2 = 10$ . The error bars are determined from multiple repeated measurements and are very small in the linear range of  $d_s$  vs  $a$ . From Figs. 3(a) and 3(b), we can see that one can manipulate the separation between trapped particles both precisely and linearly through changing the external parameter contained in the initial phase of such vortex-pair beams, and it is also better to choose a vortex-pair beam with two larger topological charge numbers for realization of a large position-controllable manipulation range between two trapped samples in practice.

For the smaller microparticles with  $d_p = 0.5\mu\text{m}$ , there may appear the optical binding effect. It is interesting and worth to further investigate how the optical binding effect impact on the optical trapping and manipulation for such structured inhomogenous focused light fields, since there maybe exist the competitive mechanism between optical

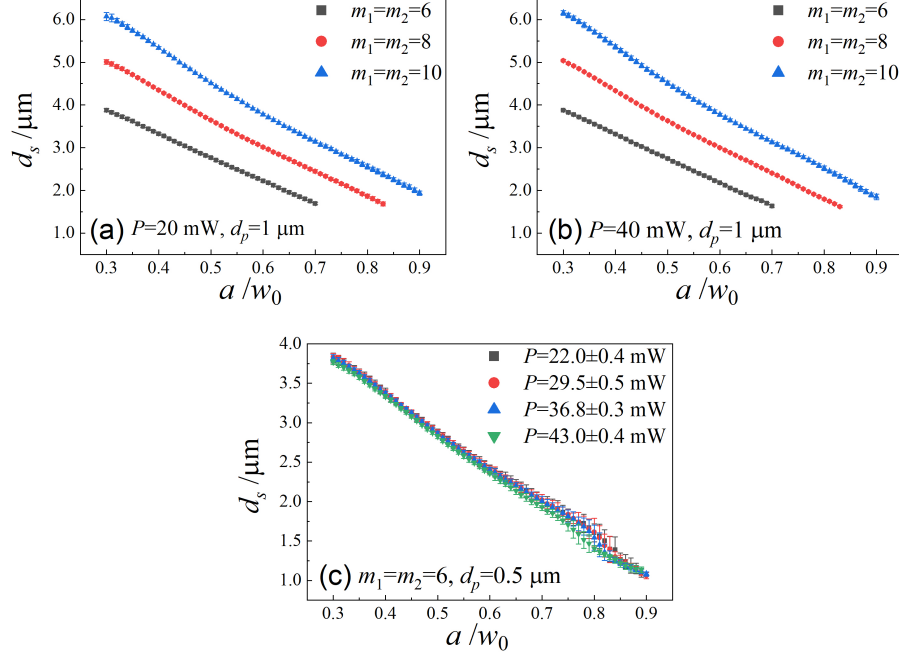


FIG. 3: Experimentally measured separation distance  $d_s$  between two trapped spherical microparticles as a function of the off-axis parameter  $a$  for different vortex-pair beams under both different incident power  $P$  and different sizes of microparticles. In (a, b) the incident power  $P$  is 20 mW and 40 mW, respectively, and the diameter of microparticles is fixed to be  $d_p = 1 \mu\text{m}$ . In (c), the values of  $m_1, m_2$  are both equal to 6,  $d_p = 0.5 \mu\text{m}$ , and the different laser power is shown in figure.

binding effect and the optical gradient forces.

In Fig. 4 we have experimentally measured the maximal magnitude of the transverse optical trapping force by the method of fluid mechanics [60]. It shows that the magnitude of the measured maximal optical trapping force increases as a function of the input laser power. When the laser power changes from 15 mW to 35 mW, the optical trapping force is roughly proportional to the power but not fully linear. Because the frictional force between the particles and the glass surface may have certain influence on the measurement since the scattering force in the propagation direction can push the particles close to the bottom surface of glass slide (note that our sample is located between the objective lens and glass slide). As the power increases, the frictional force may also increase.

It is observed from Fig. 1(b) that the initial phase structure of the vortex-pair beam is rotationally asymmetric. Therefore, naturally, this kind of beam becomes a perfect light source for controllable rotation of the trapped microparticle by rotating the beam. Experimentally, we can rotate the initial phase loaded on the SLM which is equivalent to rotate the vortex-pair beam. Figure 5 gives the experimental results on the controllable rotation of a cylindrical microrod realized by rotating the initial phase. The rotated initial phase is realized by the transform of  $\begin{cases} u' = u \cos \theta(t) + v \sin \theta(t) \\ v' = -u \sin \theta(t) + v \cos \theta(t) \end{cases}$ , which is the rotation transformation of the rectangular coordinates. The rotation angle  $\theta(t)$  can be arbitrarily designed ranged from  $0^\circ$  to  $360^\circ$ , and  $t$  represents the elapsed time of encoding the initial vortex-pair phase with different rotated angle on the SLM, and  $\bar{\omega} = \Delta\theta(t)/\Delta t$  can be the average angular speed of rotation for a vortex-pair beam, where  $\Delta\theta$  and  $\Delta t$  represent the step of the rotated angle of encoding phase image and the encoding time step, respectively, e. g., 100 images of phase distributions are designed with the rotated angle uniformly from  $0^\circ$  to  $360^\circ$ , thus  $\Delta\theta = 3.6^\circ$ , and the elapsed time for encoding 100 phase images is set to 10 s so that it means  $\Delta t = 100$  ms. In this experiment, a specially designed cylindrical microrod with length 19  $\mu\text{m}$  and diameter 4.5  $\mu\text{m}$  made of silica is used [61] and the power of the incident vortex-pair beam to the objective lens now is 35 mW. It is observed from Fig. 5(a2) that when the vortex-pair beam is rotated by  $30^\circ$ , via rotating the initial phase on SLM, the trapped cylindrical microrod is also rotated by near  $30^\circ$  as compared with the non-rotation case as seen in Fig. 5(a1). As expected, Fig. 5(a3) also shows that the rotation angle of the trapped cylindrical microrod is consistent well with the rotation angle of the initial vortex pair phase. As compared with the rotation induced by a vortex beam, this method shows high controllability, and our method also decreases the complexity of rotation with the simpler

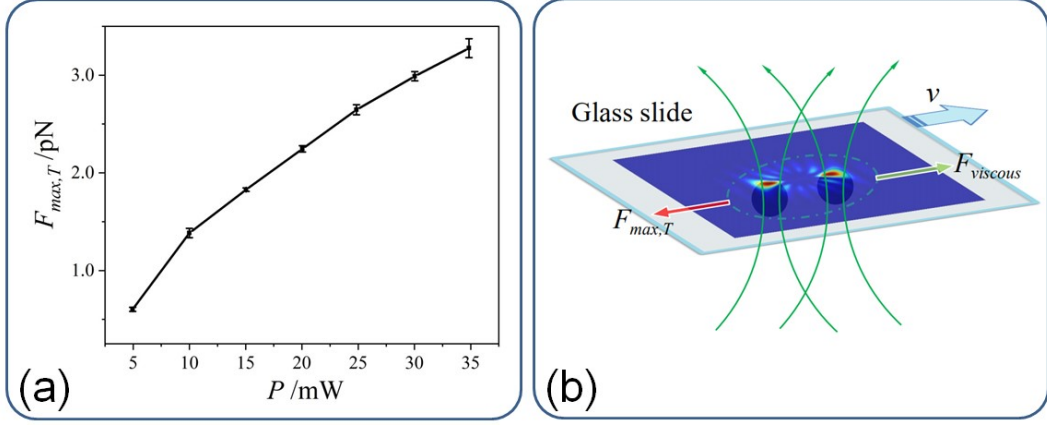


FIG. 4: (a) Experimental measurement of the maximal transverse optical trapping force of the vortex-pair beam with the same positive topological charges  $m_1 = m_2 = 6$ , the off-axis distance  $a = 0.4w_0$ , and  $w_0 = 1.5$  mm. (b) A schematic diagram to measure the maximal transverse optical force on the two microparticles. Note that the glass slide is moving from the left to right, denoted by the arrow of  $v$ , and in the horizontal direction there are mainly two opposite forces: the transverse optical force and the viscous force on microparticles. Once the speed of the glass slide increases to reach a critical value, the trapped microparticles will escape from the optical trap due to the increasing viscous force.

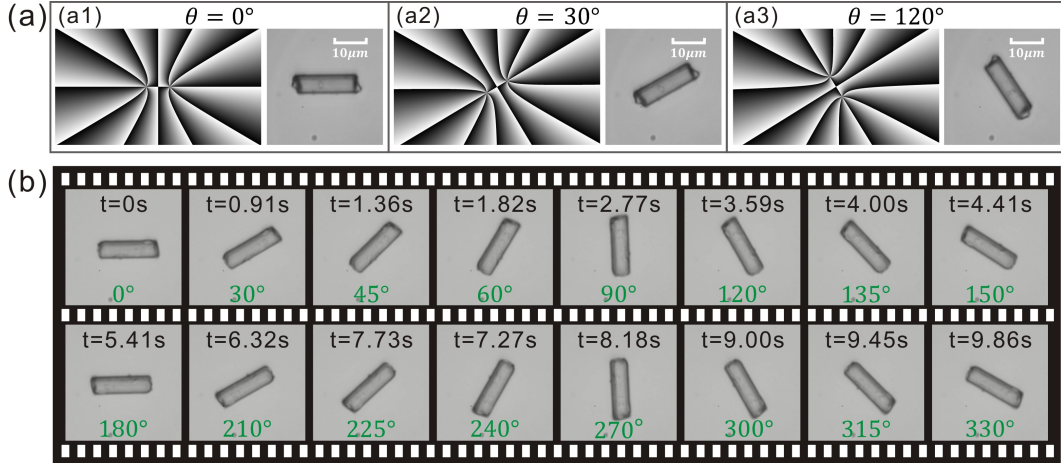


FIG. 5: Experimental realization of the angular-controllable rotation of the cylindrical microrods. (a) Rotated initial phase distributions (left) of the vortex-pair beams loaded on SLM and rotated cylindrical microrod (right) trapped by the vortex-pair beam with the specific angle (a1)  $\theta = 0^\circ$ , (a2)  $\theta = 30^\circ$ , and (a3)  $\theta = 120^\circ$ . (b) Camera snapshots of continuously rotating cylindrical microrod trapped by the vortex-pair beam with the same positive topological charges  $m_1 = m_2 = 6$ , the off-axis distance  $a = 0.6w_0$ , and  $w_0 = 1.5$  mm. The corresponding elapsing time  $t$  and the rotating angle are denoted in each snapshot, and there is a video that can be seen in Visualization 1.

experimental setup as compared with the method in Ref. [34]. Thus, it can be concluded that controllable rotation of trapping cylindrical microrod is well realized and the rotation process can be precisely controlled. Interestingly, a continuous rotation of the trapped cylindrical microrod is experimentally performed (see Visualization 1). In Fig. 5(b), a tweezed cylindrical microrod can be seen to rotate between the frames which is extracted from the video (see Visualization 1) at some typical angles. Here the average angular speed is  $\bar{\omega} \approx 36^\circ/\text{sec}$ .

In order to explain the experimental results in Figs. 2, 3, and 5, we have further measured the intensity distributions of such vortex-pair beams in a focused system, which can mimic the intensity distributions near the focal plane of the objective lens in our optical tweezers systems. Figure 6 plots the measured and numerical intensity distributions of the focused vortex-pair beams when they gradually approach to their focal point at  $s = f = 50$  cm in the  $2-f$  lens system, which is shown in inset of Fig. 1(a). Here, we want to emphasize that although there are some previous works related to the evolutions of the vortex-pair beams [45, 49–51], strictly speaking, those beams [45, 49–51] with a pair of vortices are different from our design since we have used a pure phase function given by Eq. (2) and there is no amplitude modulation in our cases. Surprisingly, little work has been done experimentally on investigating the



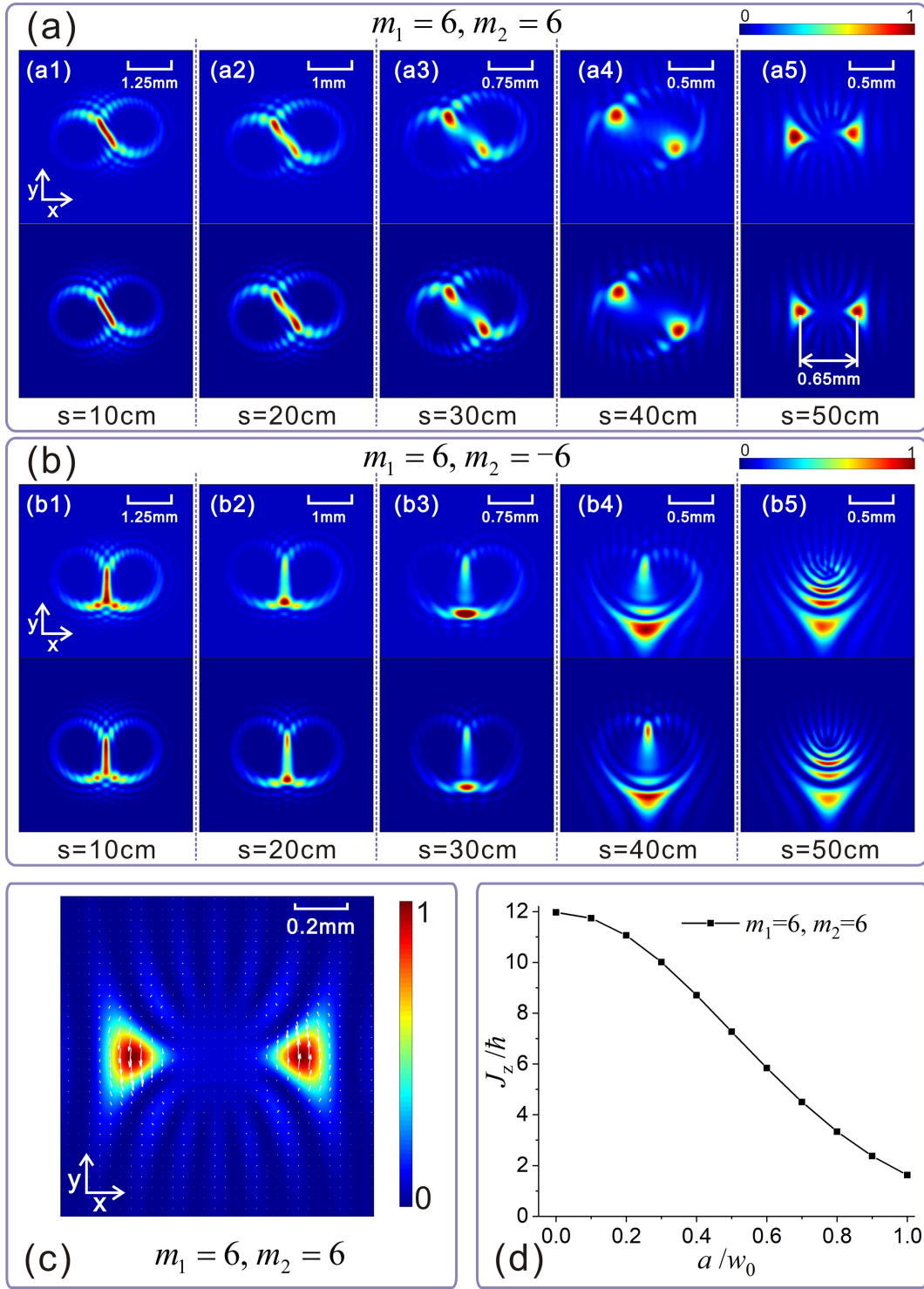


FIG. 6: The experimental (top) and numerical (bottom) results for the normalized intensity distributions of the focused vortex-pair beams with topological charges (a)  $m_1 = m_2 = 6$  and (b)  $m_1 = 6, m_2 = -6$ , at different propagation distances  $s$  in a  $2-f$  lens system under the off-axis distance  $a = 0.6w_0$ ,  $w_0 = 1.5$  mm, and  $f = 50$  cm. (c) The transverse energy flow of vortex-pair beam with topological charge  $m_1 = m_2 = 6$ . (d) The orbital angular momentum of the vortex-pair beam with  $m_1 = m_2 = 6$  as a function of the off-axis parameter  $a$ .

focusing property of such vortex-pair beams. Therefore, we have also performed the experiment to systematically demonstrate the focal evolution of the vortex-pair beam propagating in a  $2-f$  lens system, which is actually equivalent to a objective lens system in the optical trapping system. The transfer matrix of such a focal system for the inset of Fig. 1(a) is given by  $\begin{pmatrix} A & B \\ C & D \end{pmatrix} = \begin{pmatrix} 1-(s/f) & f \\ -1/f & 0 \end{pmatrix}$ . Substitute it into Eq. (3), the output light field can be obtained numerically. A lens with focal length  $f = 50$  cm is applied to our experiment. Fig. 6 shows the intensity dynamics of the vortex-pair beam with  $a = 0.6w_0$  at different propagation distances behind the lens. In Fig. 6(a1), in the case of the vortex-pair beam with two positive topological charges, there are two ring-like patterns resulted from the diffraction by the off-axis vortices at the initial phase plane, and these two ring-like patterns can interfere with each other and generate the interference patterns. As  $s$  closes to the focal point, the strongest intensity peaks gradually appear near the overlapped area where the original two ring-like patterns are overlapped. As the beam propagates to focal plane, see Figs. 6(a3)-6(a4), both two strongest spots rotate each other anticlockwise due to the role of the Gouy phase [45]. Finally, the intensity distribution becomes two main bright spots along the  $x$  axis, which is symmetric about the  $x$  and  $y$  axes, respectively. These two bright spots are very like two optical nails for catching both microparticles and microrods firmly and precisely because of the strong transverse optical gradient forces, thus the beam like an optical wrench can control the microrods precisely. When controlling the external parameters to rotate the beam generated by the SLM, one can have the operations of positioning or rotating the targets as discussed above. However, in the case of the vortex-pair beam with two opposite topological charges, as shown in Figs. 6(b1) to 6(b5), there are different behaviors for the intensity evolution due to the attractive properties of these two opposite vortices, and the intensity distribution near the focal plane simply becomes a single main bright spot with multiple curved interference fringes. Such different focal behaviors lead to the different trapping effect shown in Fig. 2. These two ring-like patterns attract each other, thus the vortex-pair beam with opposite-sign charges experiences destructive interference, and the intensity distribution at focal plane is mainly located at the  $y$  axis (which is symmetric about the  $y$  axis but not  $x$  axis). Although it can also rotate the cylindrical microrod by rotating the beam, the rotation of the cylindrical microrod is not as smooth and stable as the case of the beam with two positive topological charges (see Visualization 2). Fig. 6(c) shows the energy flow of the vortex-pair beam with topological charge  $m_1 = m_2 = 6$  at focal plane. It is observed that energy flow at right is upward while the energy flow at left is downward. Moreover, the total orbital angular momentum of the vortex-pair beam decreases as the off-axis distance  $a$  increases as shown in Fig. 6(d) which is similar to the case of a single off-axis vortex beam in Ref. [62]. However, it should be emphasized that the rotation of the microrod here is realized by rotating the vortex-pair beam with two positive topological charges based on the gradient force rather than the orbital angular momentum, since the orbital angular momentum here is weak and uncontrollable to manipulate the rotation of the particles. According to Ref. [25, 63], we have also roughly calculated the transverse gradient force of the vortex-pair beam ( $m_1 = m_2 = 6, a = 0.4w_0$ ) and the vortex beam (topological charge  $\alpha = 6$ ) under the parameter  $w_0 = 1.5$  mm,  $f = 2$  mm and input power  $P = 20$  mW at the focal plane of a  $2-f$  system which indicates that the maximum gradient force of the vortex-pair beam is about 20% higher than the vortex beam.

#### IV. CONCLUSION

In summary, we experimentally realized a kind of optical tweezers based on a single vortex-pair beam with two positive charged numbers, which provides an alternative candidate for the trapping and manipulation of microparticles and microrods. It shows that two spherical-shaped microparticles are trapped simultaneously using such kind of beams, and the separation distance between the two trapped spherical shaped microparticles can be tuned linearly by the off-axis distance of the vortex pair within the initial phase. Due to the special properties of the focused vortex-pair beam, it offers a flexible tool to simultaneously manipulate two trapped spherical microparticles and high-precisely control the orientation of the cylindrical microrods, which both can be adjusted by the external control parameters of such beams. The approach may decrease the difficulty in locating or aligning multiple microparticles and microrods since the design of vortex-pair phase is very convenient. Our results may also have potential applications in many areas like biological area and nanofabrication.

#### Acknowledgments

This work was supported by the National Natural Science Foundation of China (NSFC) (grants No.11974309 and 11674284), National Key Research and Development Program of China (No. 2017YFA0304202), Zhejiang Provincial Natural Science Foundation of China under Grant No. LD18A040001, and the Fundamental Research Funds for the



- 
- [1] Chu S, Bjorkholm JE, Ashkin A, Cable A. Experimental observation of optically trapped atoms. *Phys Rev Lett* 1986;57:314.
  - [2] Kuga T, Torii Y, Shiokawa N, Hirano T, Shimizu Y, Sasada H. Novel optical trap of atoms with a doughnut beam. *Phys Rev Lett* 1997;78:4713.
  - [3] Ashkin A, Dziedzic JM. Optical trapping and manipulation of viruses and bacteria. *Science* 1987;235:1517-20.
  - [4] Jeffries GD, Edgar JS, Zhao Y, Shelby JP, Fong C, Chiu DT. Using polarization-shaped optical vortex traps for single-cell nanosurgery. *Nano Lett* 2007;7:415-20.
  - [5] Maragò OM, Jones PH, Gucciardi PG, Volpe G, Ferrari AC, Optical trapping and manipulation of nanostructures. *Nat Nanotechnol* 2013;8:807.
  - [6] Ashkin A. Acceleration and trapping of particles by radiation pressure. *Phys Rev Lett* 1970; 24:156.
  - [7] Ashkin A, Dziedzic JM, Bjorkholm JE, Chu S. Observation of a single-beam gradient force optical trap for dielectric particles. *Opt Lett* 1986;11:288-90.
  - [8] Dufresne ER, Grier DG. Optical tweezer arrays and optical substrates created with diffractive optics. *Rev Sci Instr* 1998;69:1974-77.
  - [9] Dufresne ER, Spalding GC, Dearing MT, Sheets SA, Grier DG. Computer-generated holographic optical tweezer arrays. *Rev Sci Instr* 2001;72:1810-16.
  - [10] Curtis JE, Koss BA, Grier DG. Dynamic holographic optical tweezers. *Optics Commun* 2002;207:169-75.
  - [11] Grier DG. A revolution in optical manipulation. *Nature* 2003;424:810-16.
  - [12] Rodrigo JA, Alieva T. Freestyle 3D laser traps: tools for studying light-driven particle dynamics and beyond. *Optica* 2015;2:812-15.
  - [13] Hadad B, Froim S, Nagar H, Admon T, Eliezer Y, Roichman Y, Bahabad A. Particle trapping and conveying using an optical Archimedes' screw. *Optica* 2018;5:551-56.
  - [14] Wang XY, Zhang Q, Dai YM, Min CJ, Yuan XC. Enhancing plasmonic trapping with a perfect radially polarized beam. *Photonics Res* 2018;6:847-52.
  - [15] O'Neil AT, Macvicar I, Allen L, Padgett MJ. Intrinsic and extrinsic nature of the orbital angular momentum of a light beam. *Phys Rev Lett* 2002;88:053601.
  - [16] Curtis JE, Grier DG. Structure of optical vortices. *Phys Rev Lett* 2003; 90:133901.
  - [17] Chai HS, Wang LG. Improvement of optical trapping effect by using the focused high-order laguerre-gaussian beams. *Micron* 2012;43:887-92.
  - [18] Arlt J, Garcés-Chávez V, Sibbett W, Dholakia K. Optical micromanipulation using a Bessel light beam, *Opt Commun* 2001;197:239.
  - [19] McGloin D, Garcés-Chávez V, Dholakia K. Interfering Bessel beams for optical micromanipulation. *Opt Lett* 2003;28:657-59.
  - [20] Wang LG, Zhao CL, Wang LQ, Lu XH, Zhu SY. Effect of spatial coherence on radiation forces acting on a Rayleigh dielectric sphere. *Opt Lett* 2007;32:1393-95.
  - [21] Zhang P, Prakash J, Zhang Z, Mills MS, Efremidis NK, Christodoulides DN, Chen Z. Trapping and guiding microparticles with morphing autofocusing Airy beams. *Opt Lett* 2011; 36:2883-85.
  - [22] Daria VR, Palima DZ, Glückstad J. Optical twists in phase and amplitude. *Opt Express* 2011;19:476-81.
  - [23] Yan S, Yao B. Radiation forces of a highly focused radially polarized beam on spherical particles. *Phys Rev A* 2007;76: 053836.
  - [24] Kozawa Y, Sato S. Optical trapping of micrometer-sized dielectric particles by cylindrical vector beams. *Opt Express* 2010;18:10828-33.
  - [25] Wang LG. Optical forces on submicron particles induced by full Poincaré beams. *Opt Express* 2012;20:20814-26.
  - [26] Ambardekar AA, Li YQ. Optical levitation and manipulation of stuck particles with pulsed optical tweezers. *Opt Lett* 2005;30:1797-99.
  - [27] Wang LG, Zhao CL. Dynamic radiation force of a pulsed Gaussian beam acting on a Rayleigh dielectric sphere. *Opt Express* 2007;15:10615-21.
  - [28] Wang LG, Chai HS. Revisit on dynamic radiation forces induced by pulsed Gaussian beams. *Opt. Express* 2011;19:14389-402.
  - [29] Devi A, De AK. Theoretical investigation on nonlinear optical effects in laser trapping of dielectric nanoparticles with ultrafast pulsed excitation. *Opt, Express* 2016;24:21485-96.
  - [30] Gong LP, Gu B, Rui G, Cui YP, Zhu ZQ, Zhan QW. Optical forces of focused femtosecond laser pulses on nonlinear optical Rayleigh particles. *Photon Res* 2018;6:138-43.
  - [31] Bergamini S, Darquié B, Jones M, Jacubowicz L, Browaeys A, Grangier P. Holographic generation of microtrap arrays for single atoms by use of a programmable phase modulator. *J Opt Soc Am B* 2004;21:1889-94.
  - [32] Leonardo RD, Ianni F, Ruocco G. Computer generation of optimal holograms for optical trap arrays. *Opt. Express* 2007;15:1913-22.
  - [33] Simpson NB, Dholakia K, Allen L, Padgett MJ. Mechanical equivalence of spin and orbital angular momentum of light: an optical spanner. *Opt Lett* 1997;22:52-4.

- [34] Paterson L, MacDonald MP, Arlt J, Sibbett W, Bryant PE, Dholakia K. Controlled rotation of optically trapped microscopic particles. *Science* 2002;292:912-14.
- [35] O'Neil AT, Padgett MJ. Rotational control within optical tweezers by use of a rotating aperture. *Opt Lett* 2002;27:743-45.
- [36] Zhang DW, Yuan XC. Optical doughnut for optical tweezers. *Opt Lett* 2003;28:740-42.
- [37] Nakayama Y, Pauzauskie PJ, Radenovic A, Onorato RM, Saykally RJ, Liphardt J, Yang P. Tunable nanowire nonlinear optical probe. *Nature* 2007;447:1098-101.
- [38] Yu T, Cheong F, Sow C. The manipulation and assembly of CuO nanorods with line optical tweezers. *Nanotechnology* 2004;15:1732-36.
- [39] Gauthier RC, Ashman M, Grover CP. Experimental confirmation of the optical-trapping properties of cylindrical objects. *Appl Opt* 1999;38:4861-69.
- [40] Kreysing MK, Kießling T, Fritsch A, Dietrich C, Guck JR, Käs JA. The optical cell rotator. *Opt Express* 2008;16:16984-92.
- [41] Lee SW, Jo G, Lee T, Lee YG. Controlled assembly of In<sub>2</sub>O<sub>3</sub> nanowires on electronic circuits using scanning optical tweezers. *Optics Express* 2008;17:17491-501.
- [42] Phillips DB, Padgett MJ, Hanna S, Ho YL, Carberry DM, Miles MJ, Simpson SH. Shape-induced force fields in optical trapping. *Nature Photonics* 2014;8:400-405.
- [43] Agarwal R, Ladavac K, Roichman Y, Yu GH, Lieber CM, Grier DG. Manipulation and assembly of nanowires with holographic optical traps. *Opt Express* 2005; 13:8906-12.
- [44] Gao Y, Harder R, Southworth SH, Guest JR, Huang X, Yan Z, Pelton M. Three-dimensional optical trapping and orientation of microparticles for coherent X-ray diffraction imaging, *PNAS* 2019;16:4018-24.
- [45] Indebetouw G. Optical vortices and their propagation. *J Mod Opt* 1993;40:73-75.
- [46] Chen M, Roux FS. Accelerating the annihilation of an optical vortex dipole in a gaussian beam. *J Opt Soc Am A* 2008; 25:1279-86.
- [47] Yan H, Lü BD. Transformation of the optical vortex dipole by an astigmatic lens. *J Opt A* 2009;11:65706.
- [48] Reddy GS, Prabhakar S, Aadhi A, Banerji J, Singh RP. Propagation of an arbitrary vortex pair through an astigmatic optical system and determination of its topological charge. *J Opt Soc Am A* 2014;31:1295-302.
- [49] Chen Z, Pu JX, Zhao DM. Tight focusing properties of linearly polarized gaussian beam with a pair of vortices. *Phys Lett A* 2011;375:2958-63.
- [50] Zhao X, Pang X, Zhang J, Wan G. Transverse focal shift in vortex beams. *IEEE Photonics J* 2018;10:6500417.
- [51] He D, Gao ZH, Lü BD. Half-plane diffraction of gaussian beams carrying two vortices of equal charges. *Chin Phys B* 2011;20:104201.
- [52] Singh BK, Bahl M, Mehta DS, Senthilkumaran P. Study of internal energy flows in dipole vortex beams by knife edge test. *Opt Comm* 2013;293:15-21.
- [53] Hasegawa Y, Saitoh K, Tanaka N, Uchida M. Propagation dynamics of electron vortex pairs. *J Phys Soc Jpn* 2013;82:073402.
- [54] Collins SA. Lens-system diffraction integral written in terms of matrix optics. *J Opt Soc Am* 1970;60:1168-77.
- [55] Wang S, Zhao DM. *Matrix Optics*. Springer, 2000.
- [56] HOLOEYE Photonics AG, "Pluto-2 Phase Only Spatial Light Modulator (Reflective), device users manual," <https://holoeys.com/spatial-light-modulators/slm-pluto-phase-only/>.
- [57] Tianjing DAE Scientific CO., LTD. Type: 0.5  $\mu\text{m}$ ; Batch: 20190620; 1  $\mu\text{m}$ ; Batch: 20181219; 2  $\mu\text{m}$ ; Batch: 20190411; 3  $\mu\text{m}$ ; Batch: 20190420. Company homepage: [www.tjdaekj.com](http://www.tjdaekj.com).
- [58] Burns MM, Fournier JM, Golovchenko JA. Optical binding. *Phys Rev Lett* 1989;63:1233-36.
- [59] Ng J, Lin ZF, Chan CT, Sheng P. Photonic clusters formed by dielectric microspheres: Numerical simulations. *Phys Rev B* 2005;72:085130.
- [60] Stokes GG. On the effect of the internal friction of fluids on the motion of pendulums. Cambridge: Pitt Press, 1851.
- [61] ZiBO YI HUI NEW MATERIALS CO., LTD. Type: YHGF-1500; Batch: A190513-02. Company homepage: [ziboyi-hui.1688.com](http://ziboyi-hui.1688.com).
- [62] Kotlyar V, Kovalev A, Porfirev A, Kozlova E. Orbital angular momentum of a laser beam behind an off-axis spiral phase plate. *Opt Lett* 2019;44:3673-76.
- [63] Harada Y, Asakura T. Radiation forces on a dielectric sphere in the Rayleigh scattering regime, *Opt Commun* 1996;124:529.